Published in final edited form as:
J Thorac Oncol. 2009 December ; 4(12): 1455–1465. doi:10.1097/JTO.0b013e3181bc9419.

Induction of E-cadherin in Lung Cancer and Interaction with Growth Suppression by Histone Deacetylase Inhibition

Masatoshi Kakihana[1,2], **Tatsuo Ohira**[1,2], **Daniel Chan**[1], **Robin B. Webster**[3], **Harubumi Kato**[2], **Harry A. Drabkin**[3], and **Robert M. Gemmill**[3]

[1] Division of Medical Oncology, University of Colorado at Denver and Health Sciences Center and University of Colorado Cancer Center, Mail Stop 8117, PO Box 6511, Aurora, CO 80045-0511, USA

[2] Dept of Surgery 1, Tokyo Medical University, 6-7-1 Nishi-Shinjuku Shinjukuku, Tokyo, Japan

[3] Dept of Medicine, Hematology/Oncology, Medical Univ. of South Carolina, Charleston, SC 29425

Abstract

We previously reported that the loss of E-cadherin confers a poor prognosis in lung cancer patients and is associated with *in vitro* resistance to EGFR inhibitors. We also demonstrated that ZEB-1 is the predominant transcriptional suppressor of E-cadherin in NSCLC cell lines. We now report that treatment with MS-275, compared to vorinostat (SAHA), valproic acid or TSA, was most effective in E-cadherin up-regulation and persistence in NSCLCs. As with other tumor types and HDAC inhibitors, MS-275 inhibited growth and induced apoptosis. Importantly, blocking E-cadherin induction by shRNA resulted in less inhibition by MS-275, implicating the EMT process as a contributing factor. In contrast to H460 and H661, H157 cells were resistant to E-cadherin up-regulation by HDAC inhibitors. This resistance was overcome, in a synergistic manner, by combined knockdown of ZEB-1 and ZEB-2. In addition, H157 cells stably transfected with E-cadherin were markedly attenuated in their tumor forming ability. Lastly, combining MS-275 with the microtubule stabilizing agent, paclitaxel, or 17-AAG, an HSP 90 inhibitor, resulted in synergistic growth inhibition. Since MS-275 has no reported activity against HDAC6, which regulates both microtubule and HSP 90 functions, other mechanisms of synergy are anticipated. These results support the role of ZEB proteins and HDAC inhibitors in the pathogenesis and treatment of lung cancer.

Keywords

lung cancer; histone deacetylase; Vorinostat; E-cadherin; ZEB; 17-AAG; paclitaxel NCI-H157; NCI-H661

INTRODUCTION

Lung cancer is the leading cause of cancer deaths in the US (1,[2]). Although early detection and prevention have the potential to make a significant impact on lung cancer mortality, current approaches, e.g., helical-CT, are still controversial (3–[8]). In addition, only modest progress has been made in the treatment of locally progressed or metastatic disease. One important advance has been achieved with EGFR tyrosine kinase inhibitors, although responses are limited to a small subset of tumors with EGFR mutations or copy number increases (9,[10]). This responsive subset may also be further restricted to tumors with amplifications of eIF3H and MYC (11).

Direct correspondence to: Robert M. Gemmill., Division of Hematology/Oncology, PO Box 250635, rm 903 CSB, Jonathan Lucas St., Charleston, SC 92425, ph 843-792-4643, fax 843-792-5107, gemmill@musc.edu.

Identification of biologic factors responsible for disease pathogenesis or progression is a key strategy for development of new interventional therapeutics. We and others have shown that loss of E-cadherin in NSCLC patients is associated with a substantially increased risk of early death (12,[13]). E-cadherin loss plays a pivotal role in the transition of cells from an epithelial to mesenchymal phenotype (EMT), which is associated with increased invasion and metastases (14). In addition, we reported that E-cadherin loss is associated with resistance to EGFR inhibitors (15) and that ZEB-1 is the predominant transcriptional suppressor of E-cadherin in NSCLC cell lines (16). Of note, ZEB-1 also appears responsible for inhibiting the tumor suppressor, SEMA3F (17). As ZEB factors recruit histone deacetylase (HDAC) co-repressors, treatment with a class I/II HDAC inhibitor resulted in up-regulation of both E-cadherin (16) and SEMA3F (17). Moreover, HDAC inhibitors decreased binding of ZEB-1 to the SEMA3F promoter, at least in NCI-H661 cells.

HDAC inhibitors block cancer cell growth by multiple mechanisms including sensitizing cells to apoptosis, cell-cycle inhibition, downregulation of angiogenic factors and, as recently described, proteasome inhibition (18–[21]). HDAC inhibitors have been combined with multiple agents in human cancer cells with promising preliminary results. These agents include methylation and multi-tyrosine kinase inhibitors (22,[23]), PPARγ agonists (24), TRAIL (25), as well as single-agent (e.g., etoposide) (26) and combination chemotherapy (e.g., carboplatin plus paclitaxel) (27,[28]).

HSP90 is a chaperone that regulates the folding and stability of many proteins involved in cancer (e.g., ERB-B2, RAF, HIF-1α). In hematologic neoplasms, HDAC and HSP90 inhibitors have been successfully combined (29,[30]). However, there is little published information regarding this combination in lung cancer cells. Of note, the function of HSP90 is regulated by acetylation. Both mutations and HDAC inhibitors that affect HSP90 acetylation have been reported to inhibit the binding of client proteins, as well as other chaperones (31). While HDAC6 has a particular role in deacetylating HSP90, other HDACs also appear to be involved.

In the present study, we observed that E-cadherin was induced in NSCLC cell lines by multiple HDAC inhibitors, with the class I inhibitor, MS-275, yielding the strongest response and persistence of expression after agent removal. HDAC inhibition also reduced growth rates and induced apoptosis, as evidenced by flow cytometry and PARP cleavage. Although HDAC inhibitors have been reported to affect the expression of many hundreds of genes (32), we found that blocking the up-regulation of E-cadherin by siRNA made cells significantly more resistant to MS-275. This suggests that the observed negative effects on growth/proliferation by HDAC inhibitors stems, in part, from the EMT and especially E-cadherin. The role of ZEB-1/2 in these processes was supported by the finding that combined ZEB1/2 knockdown was necessary to restore E-cadherin in NCI-H157 cells, which are refractory to HDAC inhibitors. Moreover, E-cadherin transfectants of H157 were significantly impaired in their ability to form tumors in nude mice. Lastly, combinations of MS-275 with taxotere, or the HSP90 inhibitor, 17-AAG, resulted in synergistic growth inhibition in most NSCLC cell lines examined.

MATERIALS AND METHODS

Cell lines

Fourteen cell lines derived from NSCLC lung cancers (NCI-H157, -H290, -H292, -H322, -H460, -H513, -H647, -H661, -H1648, -H1703, -H1793, -H1299, -H2122 and A549) and two additional lines, NCI-H28 (mesothelioma) and NCI-1334 (origin unclear) were used. Cells were routinely cultured in RPMI 1640 (InVitrogen, Carlsbad, CA) supplemented with 10% FBS, 2.5% glutamine, 50,000 units penicillin and 80 μM streptomycin in a humidified 5% CO_2 atmosphere. E-cadherin-expressing variants of NCI-H157 were generated by $CaPO_4$-mediated co-transfection with pEGFP-C1 and the β-actin promoter-based expression vector

pBATEM containing human wild-type E-cadherin (33). G418 resistant colonies were expanded and sub-cloned by single cell sorting using the Flow Cytometry Core facility of the Univ. of Colorado Cancer Center.

Reagents

MS-275 (batch number: 81300002; HPLC purity, 99.82%) was supplied as a crystalline white powder by Schering AG (Berlin, Germany) while Vorinostat (SAHA) was obtained from Aton Pharma (Lot # AP-390-1, Tarrytown, NY). Both HDAC inhibitors were dissolved in DMSO at 10 mM and final DMSO concentrations in medium did not exceed 0.01%. Valproic acid (VPA), trichostatin A (TSA) and 17-(allylamino)-17-demethoxygeldanamycin (17-AAG) were purchased from Sigma (St. Louis, MO). HDAC inhibitors were used at micromolar concentrations, generally in the range of 1 to 10 μM. Treatment times were as indicated in the figure legends.

Gene knock-down

Oligonucleotides targeting CDH1 (E-cadherin), designed for expression from pSuperior.puro (OligoEngine, Inc.), were prepared from mRNA position 299 to 317 (NM_004360). Oligos were (forward) 5′-GATCCGATTGCACCGGTCGACAAATTCAAGAGATTTGTCGACCGGTGCAATCTTTTT TGGAAC and (reverse) 5′-TCGAGTTCCAAAAAAGATTGCACCGGTCGACAAATCTCTTGAATTTGTCGACCGGTG CAATCG. Mutant control oligos were (forward) 5′-GATCCGATTGCACAGGTCGACAAATTCAAGAGATTTGTCGACCTGTGCAATCTTTTT TGGAAC and (reverse) 5′-TCGAGTTCCAAAAAAGATTGCACAGGTCGACAAATCTCTTGAATTTGTCGACCTGTG CAATCG. Oligos were annealed and ligated to BglII/XhoI cleaved vector. Clones were sequence verified. NCI-H661 cells were electroporated with 1 μg of each shRNA construct and colonies selected with 3 μg/ml puromycin. Effective knock-down of E-cadherin was verified by Western blot following induction by MS-275 (Fig. 3B). For ZEB-1 and -2, pre-validated siRNAs were acquired from Invitrogen; and one with the highest knockdown efficiency and specificity for each target gene was chosen for further analysis (cat# HSS110549 for ZEB-1; # HSS190654 for ZEB-2). No significant advantage was observed with the use of more than one siRNA against the same target. Transfections were performed using HiPerFect according to manufacturer's recommendations (Qiagen, Inc.). Cells were plated at 40–60% confluency, and transfected 15h later with final concentrations of 5nM. Media were replaced at 24h and harvested for analysis at 96h post-transfection.

Total RNA was isolated using the RNAeasy kit (Qiagen, Inc.) and quantitated spectrophotometrically. Equimolar amounts were reverse-transcribed using SuperScript III First- Strand Synthesis SuperMix (Invitrogen) according to manufacturer's instructions. Real-Time detection of target cDNA was performed using 2μL of 1:5 diluted cDNA in 20 μL total reaction volumes in 96-well plates. Amplifications were analyzed on an ABI 7500 real-time PCR machine, using AmpliTaq Gold with UNG Amperase (Applied Biosystems) according to manufacturers instructions. Primer sequences were; ZEB-1_Forward, 5′-AGCAGTGAAAGAGAAGGGAATGC-3′, ZEB-1_Reverse 5′-GGTCCTCTTCAGGTGCCTCAG-3′ Reverse; ZEB-2_Forward, 5′-AACCCAAGGAGCAGGTAATCG-3′, ZEB-2_Reverse, 5′-GGAACCAGAATGGGAGAAACG-3′. Normalization primers have been described (34).

Orthotopic Nude Rat Tumorigenicity Assay

We previously documented that lung cancer cell lines grown orthotopically in nude rats had similar metastatic characteristics to that of human lung cancer patients (35,[36]). The effects of

E-cadherin on tumorigenicity and metastatic behavior of NCI-H157 cells were evaluated using this model. Six to 8-week old female athymic nude rats were obtained from the National Cancer Institute and maintained in pathogen-limited conditions at the Animal Resources Center, University of Colorado Health Sciences Center. One day prior to tumor implantation, rats were treated with 450 cGy of total body irradiation (Co^{60}) to increase immunosuppression and the subsequent rate of tumor establishment. GFP-tagged human H157 subclones (1×10^7 cells in 100μl saline) were carefully instilled into the left lung by intra-tracheal administration through a special 3 inch 22 gauge catheter (Popper & Sons, Inc., New Hyde Park, NY). Briefly, each rat was anesthetized by isofurane inhalation and held upright at 60° on a slant platform with a rubber band through its incisor teeth. The mouth cavity was opened by holding the animal's tongue and illuminated with a bright Cool-Light Source (Dolan-Jenner Industries, Lawrence, MA). Single cell suspensions were loaded into a syringe fitted with a blunt-ended Popper disposable catheter. The blunt end was also bulged so that it would not catch on and tear delicate tissues during insertion into the lungs. The catheter was inserted, bypassing the trachea and left bronchus of each animal, and cells delivered into the left lobe of the lung. The procedure was carried out aseptically and required 2 to 3 minutes per rat. Animals recovered within 5 min without casualty or showing signs of stress, were monitored for an additional 5 min, then returned to cages. Animals were monitored daily for clinical signs and body weights measured weekly. Survival was measured from the first day of tumor implantation until the end of the study (day 60 or 120). Digital pictures were taken of all lungs isolated from animals which died due to tumor burden or at the time of euthanasia, using an Olympus 2500L Digital Camera. Animal care and use was conducted in accordance with all applicable regulations and was approved by the Univ. of Colorado IACUC.

Western Blot Analysis

Following treatment, cell cultures were chilled on ice, washed twice with ice cold PBS and frozen at −80° C. Cells were disrupted in lysis buffer (20 mM Tris·HCl, pH 8.0/100 mM NaCl/ 0.5% IGEPAL/0.5 mM PMSF/10 μg/ml leupeptin/5 μg/ml pepstatin A/2.1 μg/ml aprotinin) on ice and then sonified for 15 secs. Insoluble material was removed by centrifugation (10,000g, 3 min) and protein concentrations determined by Bradford assays. Samples were mixed with Laemmli sample buffer and 10 μg aliquots resolved on SDS/PAGE gels. Following transfer to PVDF membranes (Millipore), immunodetection was carried out according to the manufacturer's instructions. Antibodies were obtained from the following sources: E-cadherin (C20820) and active-caspase 3 (# 551150) from BD Biosciences/Transduction Laboratories, (San Jose, CA), tubulin (Ab-4, NeoMarkers/LabVision, Fremont, CA), histone H4 and acetylated histone H4 (Upstate Cell Signaling Solutions, Lake Placid, NY), PARP (Cat # 1835238, Roche Applied Sciences, Indianapolis, IN), Bcl2 and ZEB-1 (Santa Cruz Biotechnology, Santa Cruz, CA). All antibodies were used at manufacturer's recommended dilutions in PBS/1% Tween (PBST) containing 1.0% nonfat dry milk. Detection used horseradish peroxidase-conjugated secondary antibodies and chemiluminescence (Western Lightning, Perkin-Elmer) or by IR fluorescence detection using a Odyssey scanner (LiCor, Lincoln, NE). Chemiluminescence signals were quantified by densitometry using a Chemi-Imager from Alpha Inotech (San Leandro, CA). Total cellular histones were purified using an acid extraction protocol provided by the anti-histone antibody supplier (Upstate, Lake Placid, NY).

MTT Cell growth assay and combination index (CI)

Growth inhibition of lung cancer cell lines was determined by the use of the colorimetric MTT cell viability assay as described previously (37). Briefly, cells were seeded in 96-well microtitre plates at 3000 cells per well (except 4000 cells/well for H290 and H2122 and 5000 cells per well for H322) and allowed to adhere overnight. Agents were added to appropriate concentrations and incubation continued for an additional 72 – 96h. MTT reagent (3- (4,5-

Dimethylthiazol-2-yl)-2,5-diphenyl-tetrazolium bromide, Sigma) was then added to 400 μg/ml and incorporated for 2–4 hours. Deposited dye was solubilized with 75% isopropanol, 240 mM HCl and absorbance measured at 490 nm in a 96-well plate reader (Molecular Devices, Inc.). The combination index (CI) was calculated by CALCUSYN (38). CI values <1.0 suggested synergy, values = 1.0 indicated additivity while values > 1.0 suggested antagonism.

Apoptosis quantitation by YO-PRO-1 staining

Apoptosis was assessed by *in situ* staining using the Vybrant apoptosis assay kit #4 (Molecular Probes, Eugene, OR). This method relies on the DNA-binding and membrane-impermeable green fluorescent dye, YO-PRO-1 (39). Following treatments, cells were washed, resuspended in 1.0 ml of PBS, and 1 μl/ml YO-PRO-1 and propidium iodide (PI) were added. Cells were incubated for 30 min on ice and then analyzed by flow cytometry (FACScan; Becton Dickinson, Franklin Lakes, NJ) through the Univ. of Colorado Flow Cytometry Core facility. Fluorescence emissions were monitored at 530 nm (YO-PRO-1 = apoptotic) and 575 nm (PI = necrotic). The Apoptotic Index was calculated as the number of apoptotic cells/total cells (10,000 minimum). Data were analyzed using CellQuest software (Becton Dickinson). All observations were reproduced at least three times in independent experiments.

Statistical methods

IC50 values and standard deviations were estimated using linear interpolation between the doses about the 50% inhibition point. Combination index values were obtained using the methods of Chou and Talalay (24). Survival curves were obtained using the method of Kaplan and Meier (40). A two-way analysis of variance with interaction was used to compare growth inhibition between control and knock-down cells across doses of MS-275. Post-hoc comparisons using Tukey's HSD were applied at each dose to compare growth across groups. All hypothesis tests were performed at the 0.05 level of significance.

RESULTS

E-cadherin is induced by multiple HDAC inhibitors

We previously reported that the HDAC inhibitor trichostatin A (TSA) induced E-cadherin in the NSCLC cell lines, NCI-H661 and NCI-H460 (16). To extend these results, we compared several HDAC inhibitors for their ability to up-regulate E-cadherin over time. Cells were treated with indicated doses of trichostatin A (TSA), valproic acid (VPA), benzamide (MS-275) or vorinostat (VOR; suberoylanilide hydroxamic acid/saha), and protein lysates analyzed by Western blot. As can be seen in Fig. 1A, E-cadherin induction and persistence differed in a cell line and agent-dependent fashion, with the highest levels consistently observed at 24h. A dose-response analysis demonstrated that H661 cells were highly responsive to both MS-275 and vorinostat (Fig. 1B), even at 1 μM. When H661 cells were pre-treated with MS-275 for 12h, then drug was washed away, E-cadherin persisted for 4 days while TSA effects were lost after 24 h (Fig. 1C). Acetylated histone H4 accumulation verified efficacy of HDAC inhibitors (Fig 1D).

Growth inhibition by HDAC inhibitors is dependent, in part, upon E-cadherin induction

HDAC inhibitors have been reported to block growth of lung cancer cell lines (41). Growth inhibition by MS-275 was verified in 12 NSCLC cell lines using MTT assays. Inhibition curves are shown for three representative lines in Fig. 2 while corresponding IC_{50} values for all lines are listed in Table 1. Similar to reports using vorinostat treatment, we observed IC_{50} values for MS-275 ranging from less than 0.3 μM (H2122) to approximately 10 μM (H322).

We previously reported that loss of E-cadherin (or β-catenin) was a poor prognostic factor in lung cancer (12). Moreover, transfected E-cadherin suppressed in vitro growth and sensitized NCI-H157 cells to the EGFR inhibitor, gefitinib (15). To determine if E-cadherin induction contributed to the anti-proliferative effects of HDAC inhibition, we stably knocked-down E-cadherin (CDH1) mRNA in H661 cells with a shRNA construct, using a non-targeting shRNA as control. E-cadherin was induced by MS-275 (at 1, 2.5 and 5 μM) in control cells after 24h (Fig. 3A, left panel), while induction was substantially blunted in CDH1 knock-down cells (right panel). Differential effects on growth inhibition were then assessed by MTT assays (Fig. 3B). Specific reduction of E-cadherin increased the resistance to growth inhibition by MS-275 at both 2 and 4 μM, and the latter was statistically significant ($p = 0.001$, Tukey's HSD test). These results suggest that induction of E-cadherin contributes to the growth inhibition of NSCLC cells mediated by MS-275 and probably other HDAC inhibitors.

ZEB-1/2-dependent but HDAC class I/II independent suppression of E-cadherin

Our previous work showed that ZEB-1 was the predominant transcriptional repressor of E-cadherin in NSCLC cell lines (15,[16]). ZEB recruits the co-repressor CtBP (14), which complexes with several HDACs including HDAC1/2 (class I) and HDACs 4 and 7 (class II) (42). While testing HDAC inhibitor effects, we discovered that H157 cells were resistant to E-cadherin upregulation at both the protein (Fig. 4A) and mRNA levels (not shown). To determine whether ZEB was responsible for E-cadherin repression in this line, we knocked-down ZEB-1 and ZEB-2 (SIP1/Zfhx1B), separately or together, and analyzed CDH1 mRNA and E-cadherin protein. As shown in Fig. 4B, individual knock-downs of ZEB-1 or ZEB-2 led to modest increases in E-cadherin mRNA, but this was insufficient to detect E-cadherin protein (Fig 4C). However, the combined knock-down of ZEB-1 and ZEB-2 led to a ~1000-fold increase in E-cadherin mRNA and robust expression of E-cadherin protein (lane 6). Thus, E-cadherin suppression in H157 cells is ZEB-dependent, but independent of class I/II HDAC enzymes (see Discussion). Several additional lines expressing low to no E-cadherin (15) were treated with TSA and MS-275 to determine if resistance to HDAC inhibitors was unique to H157 cells. MS-275 increased mature E-cadherin (120 kDa) in H2122 cells but two other lines were resistant (Fig 4A). Thus HDACi treatments may restore E-cadherin in approximately one-half of negative tumors.

E-cadherin blocks tumorigenicity of NCI-H157 cells

H157 cells form aggressive tumors in an orthotopic *nude* rat model. To test the effects of E-cadherin expression on tumorigenicity, H157 cells were stably co-transfected with an E-cadherin expression vector together with a GFP vector carrying G418 resistance (Fig. 5A). Two independent transfectants (E1 and E6) were examined. Tumors developed rapidly from H157/GFP control cells and metastasized to the right lung and mediastinal lymph nodes (Fig. 5B, left, black arrowhead). However, tumor formation was suppressed by re-expression of E-cadherin. After nearly 4 months, H157/E6 cells yielded only small primary tumors (white arrowhead). Kaplan-Meier survival statistics confirmed the aggressive nature of H157/GFP control tumors while most animals survived beyond 60 days when E-cadherin was re-expressed (Fig. 5C).

Combining the HDAC inhibitor, MS-275, with 17-AAG or taxotere results in synergistic growth inhibition

We then examined the addition of a proteasome inhibitor, PS341 (Bortezomid), Hsp90 inhibitor, 17-AAG [17-(allylamino)-17-demethoxygeldanamycin] (43), or a microtubule-targeting agent, taxotere, to determine if these would enhance the anti-proliferative effects of MS-275. The combination with PS341 proved inconsistent and was not further studied.

However, the addition of either 17-AAG or taxotere resulted in consistent synergistic growth inhibition in most lines.

As a single agent, 17-AAG inhibited growth with IC_{50} values ranging between 20–300 nm. With MS-275, the combination index (CI) values ranged between 0.3 and 0.8 (Table 2), indicative of synergy. In H322 cells, which were relatively resistant to MS-275, the addition of 17-AAG increased the sensitivity to the HDAC inhibitor by approximately 10-fold. However, this was cell line-dependent, since the combination was antagonistic in H1793 cells and only a modest change in sensitivity was observed in A549. Similar results were obtained with taxotere. As a single agent, taxotere inhibited growth in all cell lines with IC_{50} values ranging from 2 to 65 nM. The combination resulted in synergistic growth inhibition, with CI values ranging from 0.08 to 0.55 (Table 3). Peak synergistic interactions with MS-275 were frequently observed at taxotere levels of one-half to one-third of individual IC_{50} values. Notably, the three most resistant lines to MS-275 demonstrated a 10 to 20-fold increased sensitivity upon addition of taxotere.

Treatment with HDAC inhibitors led to morphological changes consistent with apoptosis and detachment from substrate. YO-PRO1 staining and flow cytometry were used to quantify apoptotic effects in ten lines following treatment with either trichostatin A (TSA, 0.33 μM) or MS-275 (10 μM). TSA induced early apoptosis (YO-PRO1-positive) in about 60% of H661 cells after 48 h (Fig. 6B). Similarly, 36% of H290 cells underwent apoptosis with MS-275 (Fig. 6D). The percent of apoptotic cells treated with MS-275 at their IC_{50} for 24 h is shown in Table 1. Additional evidence of apoptosis was obtained using activated caspase-3 and cleaved poly ADP ribose polymerase (PARP), as shown for NCI-H647 cells (Fig. 6E), which were moderately sensitive to MS-275 in terms of growth inhibition. In contrast, resistant A549 cells showed little caspase activation and lower levels of cleaved PARP. Similar results were obtained using either variable doses for 36 h or a single dose (5 μM) over a 2 day time course (Fig. 6F).

There was no apparent correlation between the observed growth inhibition (using MTT assays at 72–96h) and apoptosis (performed after 24h of treatment), i.e., Spearman $r = -0.244$, $p=0.56$. This suggests that the mechanism of growth inhibition by HDAC inhibitors includes factors in addition to apoptosis. In support of this, we also examined Bcl-2 levels by Western blot (Fig. 6G) and compared the densitometry measurements with growth inhibition by MS-275. No significant correlation was detected, i.e., Spearman $r = -0.049$; $p = 0.879$, and some resistant lines (e.g., A549, H1793) expressed lower Bcl-2 levels than sensitive ones (e.g., H647). Thus, together with the YO-PRO1 staining, we conclude that these assessments of apoptosis and Bcl-2 levels do not significantly correlate with growth inhibition by MS-275 (as a single agent).

DISCUSSION

E-cadherin loss is associated with enhanced invasion and metastases in many epithelial-derived tumors (12,[44]–[48]). In lung cancer, we previously reported that reduced E-cadherin was associated with loss of differentiation, increased invasion and metastasis as well as reduced survival (12). Among other transcriptional repressors in lung cancer cell lines, we found that ZEB-1 levels best correlated with reduced E-cadherin expression and that blocking ZEB-1 with either siRNA or the class I/II HDAC inhibitor, TSA, resulted in E-cadherin upregulation (16). We began our present studies with the goal of comparing different HDAC inhibitors for their ability to up-regulate E-cadherin in NSCLC cells lines. MS-275, a class I HDAC inhibitor (49), resulted in the largest induction and persistance of E-cadherin compared to TSA, valproic acid and vorinostat (Fig. 1). MS-275 inhibited the growth of NSCLC cell lines (Fig. 2, Table 1), similar to numerous reports with HDAC inhibitors in other tumors. However, whether the upregulation of E-cadherin plays any role in this process had not been investigated to our

knowledge. Importantly, we found that blocking upregulation of E-cadherin by siRNA partially relieved the growth suppression due to single-agent MS-275 (Fig. 3). There are several possible mechanisms how this might occur, which include among others effects on intercellular adhesion, cell-cycle regulation and associated changes in growth factor signaling during epithelial-mesenchymal transition. Although more work will be required to elucidate the responsible pathway(s), which may be context specific, we conclude that E-cadherin has a distinct role in growth inhibition mediated by HDAC inhibitors and that strategies to upregulate E-cadherin might be additive or synergistic with other biologic-based therapies to block tumor growth.

E-cadherin was induced by MS-275 in H2122, H460 and H661 cells, and by VPA, TSA and vorinostat in the latter two lines, while none of these agents were effective in H157, H1299 or H1703 (Fig. 4A). Mechanistically, these results suggest that HDACs recruited by transcriptional repressors like ZEB-1/2 are responsible for E-cadherin suppression in about one-half of those NSCLCs negative for this epithelial adhesion molecule.

Interestingly, individual knockdowns of ZEB-1 or ZEB-2 in H157 cells resulted only in modest up-regulation of E-cadherin mRNA (Fig. 4B, note $\log_{10}$ scale) without any observable protein accumulation (Fig. 4C, lanes 3–5). In contrast, the simultaneous knockdown of ZEB-1 and ZEB-2 resulted in synergistic E-cadherin mRNA upregulation (>1000-fold) and marked protein expression (lane 6). These results emphasize the importance of ZEB-1 and -2, even when class I/II HDACs are not apparently involved, and suggest that the two ZEB orthologs are not merely functionally redundant. Such cooperativity might occur, for example, if each factor recruited different components to the E-cadherin promoter, which together resulted in less accessibility of the DNA than either factor alone. Alternatively, ZEB-1 and -2 may bind distinct E-cadherin regulatory sites. The lack of response to class HDAC I/II inhibitors may also be due to the involvement of a class III enzyme (50). However, we do not know at present whether the inhibition is CtBP-dependent or might result from another suppressive mechanism (51). In H661 cells, we observed displacement of ZEB-1 from the SEMA3F promoter upon treatment with vorinostat (17). In H157 cells, our observation that E-cadherin silencing is ZEB-dependent but class I/II HDAC independent implies that ZEB factor displacement may be cell line specific and/or may depend upon the specific HDACs recruited.

Up-regulation of E-cadherin in H157 cells had a potent effect on *in vivo* tumorigenicity. As shown in Fig. 5, two clones of H157 cells stably expressing comparable amounts of E-cadherin were markedly attenuated in their ability to form tumors when injected orthotopically into the lungs of nude rats. These results validate the tumor suppressing contribution made by E-cadherin in NSCLC.

There are numerous pre-clinical and clinical reports examining the effects of HDAC inhibitors alone and in combination with other agents (22–[28,52]). HDAC inhibitors selectively induce apoptosis in cancer cells through changes in levels and activities of pro- and anti-apoptotic proteins, stress kinases, reactive oxygen species and, as recently described, from inhibition of proteasome function (21,[53–56]). As expected, single-agent MS-275 induced apoptosis in NSCLC cells, as evidenced by Annexin V staining, PARP cleavage and caspase 3 activation (Fig. 6A–F).

In limited experiments, we explored the combination of MS-275 with either paclitaxel, a microtubule stabilizing agent, or 17-AAG, an inhibitor of HSP90. With paclitaxel, synergistic growth inhibition was observed (Table 3). Taxols inhibit microtubule function and induce apoptosis in a caspase-dependent manner (57). In addition, microtubule function is regulated in part by acetylation, with the class II enzyme, HDAC6, being an important microtubule deacetylase. However, MS-275 has no *in vitro* activity against HDAC6 (49), implying that

there must be a different mechanism of action to explain the synergy. The combination of HDAC and HSP 90 inhibitors has been less well studied. In leukemia cells, the class I/II inhibitor, vorinostat, enhanced the anti-tumor activity of 17-AAG reportedly through its activity against HDAC6, which removes acetyl groups from HSP90 enhancing its function (30). In addition, HDAC6 was shown to be an HSP90 client protein. We observed that MS-275 plus 17-AAG synergistically inhibited growth in most NSCLC cell lines (Table 2). As with paclitaxel, the expected mechanism of synergy should be other than HDAC6 inhibition, although we do not know if it is affected indirectly. Lastly, one further observation is that neither the presence of apoptosis nor BCL-2 levels significantly correlated with the degree of growth inhibition (Table 1), which would be consistent with a multi-factorial explanation for the anti-growth properties of these agents.

In conclusion, we found that MS-275 was the most effective HDAC inhibitor to up-regulate E-cadherin in these NSCLC cell lines. Furthermore, E-cadherin up-regulation appears to play a role in HDAC inhibitor-mediated growth inhibition and, when stably transfected, has a potent *in vivo* anti-tumor effect. The results presented here also confirm our previous findings concerning the predominant role played by ZEB proteins in E-cadherin transcriptional repression in NSCLC cell lines. Moreover, ZEB-1 and ZEB-2 can contribute in a synergistic manner to E-cadherin suppression and, in some cases, their effects are independent of class I/II HDACs, a finding which has potential therapeutic importance. Lastly, the combination of MS-275 with either paclitaxel or an HSP 90 inhibitor appears promising.

Acknowledgments

We thank J. Jacobsen and J. Nair-Menon for maintenance of tissue cultures and assistance with selected experimentation, B. Helfrich for assistance with MTT assays and the Univ. of Colorado Cancer Center Flow Cytometry and Animal Resource Cores, supported by NCI-CA46934. This work was supported by a Lung Cancer SPORE grant (NCI-CA58187).

Abbreviations

TSA	trichostatin A
MS-275	benzamide
VPA	valproic acid
SAHA	vorinostat, suberoylanilide hydroxamic acid
17-AAG	17-(allylamino)-17-demethoxygeldanamycin
GFP	green fluorescent protein
PMSF	phenylmethylsulfonylfluride
HDAC	histone deacetylase

References

1. Jemal A, Siegel R, Ward E, et al. Cancer statistics. CA Cancer J Clin 2006;56(2):106–30. [PubMed: 16514137]
2. Parkin DM, Bray F, Ferlay J, Pisani P. Global cancer statistics, 2002. CA Cancer J Clin 2005;55(2): 74–108. [PubMed: 15761078]
3. Henschke CI, Yankelevitz DF, Libby DM, Pasmantier MW, Smith JP, Miettinen OS. Survival of patients with stage I lung cancer detected on CT screening. The New England journal of medicine 2006;355(17):1763–71. [PubMed: 17065637]

4. Welch HG, Woloshin S, Schwartz LM, et al. Overstating the evidence for lung cancer screening: the International Early Lung Cancer Action Program (I-ELCAP) study. Archives of internal medicine 2007;167(21):2289–95. [PubMed: 18039986]
5. Sone S, Nakayama T, Honda T, et al. CT findings of early-stage small cell lung cancer in a low-dose CT screening programme. Lung cancer (Amsterdam, Netherlands) 2007;56(2):207–15.
6. Sone S, Nakayama T, Honda T, et al. Long-term follow-up study of a population-based 1996–1998 mass screening programme for lung cancer using mobile low-dose spiral computed tomography. Lung cancer (Amsterdam, Netherlands) 2007;58(3):329–41.
7. Roberts HC, Patsios D, Paul NS, et al. Lung cancer screening with low-dose computed tomography: Canadian experience. Canadian Association of Radiologists journal = Journal l'Association canadienne des radiologistes 2007;58(4):225–35. [PubMed: 18186434]
8. Wilson DO, Weissfeld JL, Fuhrman CR, et al. The Pittsburgh Lung Screening Study (PLuSS): outcomes within 3 years of a first computed tomography scan. American journal of respiratory and critical care medicine 2008;178(9):956–61. [PubMed: 18635890]
9. Cappuzzo F, Hirsch FR, Rossi E, et al. Epidermal growth factor receptor gene and protein and gefitinib sensitivity in non-small-cell lung cancer. Journal of the National Cancer Institute 2005;97(9):643–55. [PubMed: 15870435]
10. Lynch TJ, Bell DW, Sordella R, et al. Activating mutations in the epidermal growth factor receptor underlying responsiveness of non-small-cell lung cancer to gefitinib. The New England journal of medicine 2004;350(21):2129–39. [PubMed: 15118073]
11. Cappuzzo F, Varella-Garcia M, Rossi E, et al. MYC and EIF3H Coamplification Significantly Improve Response and Survival of Non-small Cell Lung Cancer Patients (NSCLC) Treated with Gefitinib. J Thorac Oncol. 2009
12. Bremnes RM, Veve R, Gabrielson E, et al. High-throughput tissue microarray analysis used to evaluate biology and prognostic significance of the E-cadherin pathway in non-small-cell lung cancer. J Clin Oncol 2002;20(10):2417–28. [PubMed: 12011119]
13. Hidaka N, Nagao T, Asoh A, Kondo Y, Nagao K. Expression of E-cadherin, alpha-catenin, beta-catenin, and gamma-catenin in bronchioloalveolar carcinoma and conventional pulmonary adenocarcinoma: an immunohistochemical study. Mod Pathol 1998;11(11):1039–45. [PubMed: 9831199]
14. Peinado H, Olmeda D, Cano A. Snail, Zeb and bHLH factors in tumour progression: an alliance against the epithelial phenotype? Nat Rev Cancer 2007;7(6):415–28. [PubMed: 17508028]
15. Witta SE, Gemmill RM, Hirsch FR, et al. Restoring E-cadherin expression increases sensitivity to epidermal growth factor receptor inhibitors in lung cancer cell lines. Cancer Res 2006;66(2):944–50. [PubMed: 16424029]
16. Ohira T, Gemmill RM, Ferguson K, et al. WNT7a induces E-cadherin in lung cancer cells. Proceedings of the National Academy of Sciences of the United States of America 2003;100(18):10429–34. [PubMed: 12937339]
17. Clarhaut J, Gemmill RM, Potiron VA, et al. ZEB-1, a Repressor of the semaphorin 3F tumor suppressor gene in lung cancer cells. Neoplasia 2009;11(2):157–66. [PubMed: 19177200]
18. Qian DZ, Kato Y, Shabbeer S, et al. Targeting tumor angiogenesis with histone deacetylase inhibitors: the hydroxamic acid derivative LBH589. Clin Cancer Res 2006;12(2):634–42. [PubMed: 16428510]
19. Deroanne CF, Bonjean K, Servotte S, et al. Histone deacetylases inhibitors as anti-angiogenic agents altering vascular endothelial growth factor signaling. Oncogene 2002;21(3):427–36. [PubMed: 11821955]
20. Minucci S, Pelicci PG. Histone deacetylase inhibitors and the promise of epigenetic (and more) treatments for cancer. Nat Rev Cancer 2006;6(1):38–51. [PubMed: 16397526]
21. Fotheringham S, Epping MT, Stimson L, et al. Genome-wide loss-of-function screen reveals an important role for the proteasome in HDAC inhibitor-induced apoptosis. Cancer cell 2009;15(1):57–66. [PubMed: 19111881]
22. Zhu WG, Otterson GA. The interaction of histone deacetylase inhibitors and DNA methyltransferase inhibitors in the treatment of human cancer cells. Current medicinal chemistry 2003;3(3):187–99. [PubMed: 12769777]

23. Yu C, Friday BB, Lai JP, et al. Abrogation of MAPK and Akt signaling by AEE788 synergistically potentiates histone deacetylase inhibitor-induced apoptosis through reactive oxygen species generation. Clin Cancer Res 2007;13(4):1140–8. [PubMed: 17317822]
24. Chang TH, Szabo E. Enhanced growth inhibition by combination differentiation therapy with ligands of peroxisome proliferator-activated receptor-gamma and inhibitors of histone deacetylase in adenocarcinoma of the lung. Clin Cancer Res 2002;8(4):1206–12. [PubMed: 11948134]
25. Ziauddin MF, Yeow WS, Maxhimer JB, et al. Valproic acid, an antiepileptic drug with histone deacetylase inhibitory activity, potentiates the cytotoxic effect of Apo2L/TRAIL on cultured thoracic cancer cells through mitochondria-dependent caspase activation. Neoplasia 2006;8(6):446–57. [PubMed: 16820090]
26. Hajji N, Wallenborg K, Vlachos P, Nyman U, Hermanson O, Joseph B. Combinatorial action of the HDAC inhibitor trichostatin A and etoposide induces caspase-mediated AIF-dependent apoptotic cell death in non-small cell lung carcinoma cells. Oncogene 2008;27(22):3134–44. [PubMed: 18071312]
27. Ramalingam SS, Parise RA, Ramanathan RK, et al. Phase I and pharmacokinetic study of vorinostat, a histone deacetylase inhibitor, in combination with carboplatin and paclitaxel for advanced solid malignancies. Clin Cancer Res 2007;13(12):3605–10. [PubMed: 17510206]
28. Pauer LR, Olivares J, Cunningham C, et al. Phase I study of oral CI-994 in combination with carboplatin and paclitaxel in the treatment of patients with advanced solid tumors. Cancer investigation 2004;22(6):886–96. [PubMed: 15641487]
29. George P, Bali P, Annavarapu S, et al. Combination of the histone deacetylase inhibitor LBH589 and the hsp90 inhibitor 17-AAG is highly active against human CML-BC cells and AML cells with activating mutation of FLT-3. Blood 2005;105(4):1768–76. [PubMed: 15514006]
30. Rao R, Fiskus W, Yang Y, et al. HDAC6 inhibition enhances 17-AAG--mediated abrogation of hsp90 chaperone function in human leukemia cells. Blood 2008;112(5):1886–93. [PubMed: 18591380]
31. Scroggins BT, Robzyk K, Wang D, et al. An acetylation site in the middle domain of Hsp90 regulates chaperone function. Molecular cell 2007;25(1):151–9. [PubMed: 17218278]
32. Peart MJ, Smyth GK, van Laar RK, et al. Identification and functional significance of genes regulated by structurally different histone deacetylase inhibitors. Proceedings of the National Academy of Sciences of the United States of America 2005;102(10):3697–702. [PubMed: 15738394]
33. Handschuh G, Candidus S, Luber B, et al. Tumour-associated E-cadherin mutations alter cellular morphology, decrease cellular adhesion and increase cellular motility. Oncogene 1999;18(30):4301–12. [PubMed: 10439038]
34. Vandesompele J, De Preter K, Pattyn F, et al. Accurate normalization of real-time quantitative RT-PCR data by geometric averaging of multiple internal control genes. Genome biology 2002;3(7):1–12.
35. Chan DC, Earle KA, Zhao TL, et al. Exisulind in combination with docetaxel inhibits growth and metastasis of human lung cancer and prolongs survival in athymic nude rats with orthotopic lung tumors. Clin Cancer Res 2002;8(3):904–12. [PubMed: 11895925]
36. Kusy S, Nasarre P, Chan D, et al. Selective suppression of in vivo tumorigenicity by semaphorin SEMA3F in lung cancer cells. Neoplasia 2005;7(5):457–65. [PubMed: 15967098]
37. Gemmill RM, Zhou M, Costa L, Korch C, Bukowski RM, Drabkin HA. Synergistic growth inhibition by Iressa and Rapamycin is modulated by VHL mutations in renal cell carcinoma. British Journal of Cancer 2005;92(12):2266–77. [PubMed: 15956968]
38. Chou TC, Talalay P. Quantitative analysis of dose-effect relationships: the combined effects of multiple drugs or enzyme inhibitors. Adv Enzyme Regul 1984;22:27–55. [PubMed: 6382953]
39. Idziorek T, Estaquier J, De Bels F, Ameisen JC. YOPRO-1 permits cytofluorometric analysis of programmed cell death (apoptosis) without interfering with cell viability. J Immunol Methods 1995;185(2):249–58. [PubMed: 7561136]
40. Kaplan EL, Meier P. Nonparametric estimation from incomplete observations. J Am Stat Assoc 1958;53:457–81.
41. Miyanaga A, Gemma A, Noro R, et al. Antitumor activity of histone deacetylase inhibitors in non-small cell lung cancer cells: development of a molecular predictive model. Molecular cancer therapeutics 2008;7(7):1923–30. [PubMed: 18606719]

42. Chinnadurai G. Transcriptional regulation by C-terminal binding proteins. The international journal of biochemistry & cell biology 2007;39(9):1593–607.
43. Neckers L. Using natural product inhibitors to validate Hsp90 as a molecular target in cancer. Curr Top Med Chem 2006;6(11):1163–71. [PubMed: 16842153]
44. Bohm M, Totzeck B, Birchmeier W, Wieland I. Differences of E-cadherin expression levels and patterns in primary and metastatic human lung cancer. Clin Exp Metastasis 1994;12(1):55–62. [PubMed: 8287621]
45. Kase S, Sugio K, Yamazaki K, Okamoto T, Yano T, Sugimachi K. Expression of E-cadherin and beta-catenin in human non-small cell lung cancer and the clinical significance. Clin Cancer Res 2000;6(12):4789–96. [PubMed: 11156236]
46. Liu D, Huang C, Kameyama K, et al. E-cadherin expression associated with differentiation and prognosis in patients with non-small cell lung cancer. Ann Thorac Surg 2001;71(3):949–54. discussion 54–5. [PubMed: 11269479]
47. Takeichi M. Cadherin cell adhesion receptors as a morphogenetic regulator. Science (New York, NY 1991;251(5000):1451–5.
48. Cowin P, Rowlands TM, Hatsell SJ. Cadherins and catenins in breast cancer. Curr Opin Cell Biol 2005;17(5):499–508. [PubMed: 16107313]
49. Khan N, Jeffers M, Kumar S, et al. Determination of the class and isoform selectivity of small-molecule histone deacetylase inhibitors. The Biochemical journal 2008;409(2):581–9. [PubMed: 17868033]
50. Pruitt K, Zinn RL, Ohm JE, et al. Inhibition of SIRT1 reactivates silenced cancer genes without loss of promoter DNA hypermethylation. PLoS genetics 2006;2(3):e40. [PubMed: 16596166]
51. van Grunsven LA, Michiels C, Van de Putte T, et al. Interaction between Smad-interacting protein-1 and the corepressor C-terminal binding protein is dispensable for transcriptional repression of E-cadherin. The Journal of biological chemistry 2003;278(28):26135–45. [PubMed: 12714599]
52. Marks PA, Breslow R. Dimethyl sulfoxide to vorinostat: development of this histone deacetylase inhibitor as an anticancer drug. Nat Biotechnol 2007;25(1):84–90. [PubMed: 17211407]
53. Jaboin J, Wild J, Hamidi H, et al. MS-27-275, an inhibitor of histone deacetylase, has marked in vitro and in vivo antitumor activity against pediatric solid tumors. Cancer Res 2002;62(21):6108–15. [PubMed: 12414635]
54. Rosato RR, Almenara JA, Grant S. The histone deacetylase inhibitor MS-275 promotes differentiation or apoptosis in human leukemia cells through a process regulated by generation of reactive oxygen species and induction of p21CIP1/WAF1 1. Cancer Res 2003;63(13):3637–45. [PubMed: 12839953]
55. Lucas DM, Davis ME, Parthun MR, et al. The histone deacetylase inhibitor MS-275 induces caspase-dependent apoptosis in B-cell chronic lymphocytic leukemia cells. Leukemia 2004;18(7):1207–14. [PubMed: 15116122]
56. Dai Y, Rahmani M, Dent P, Grant S. Blockade of histone deacetylase inhibitor-induced RelA/p65 acetylation and NF-kappaB activation potentiates apoptosis in leukemia cells through a process mediated by oxidative damage, XIAP downregulation, and c-Jun N-terminal kinase 1 activation. Molecular and cellular biology 2005;25(13):5429–44. [PubMed: 15964800]
57. Wang TH, Wang HS, Soong YK. Paclitaxel-induced cell death: where the cell cycle and apoptosis come together. Cancer 2000;88(11):2619–28. [PubMed: 10861441]

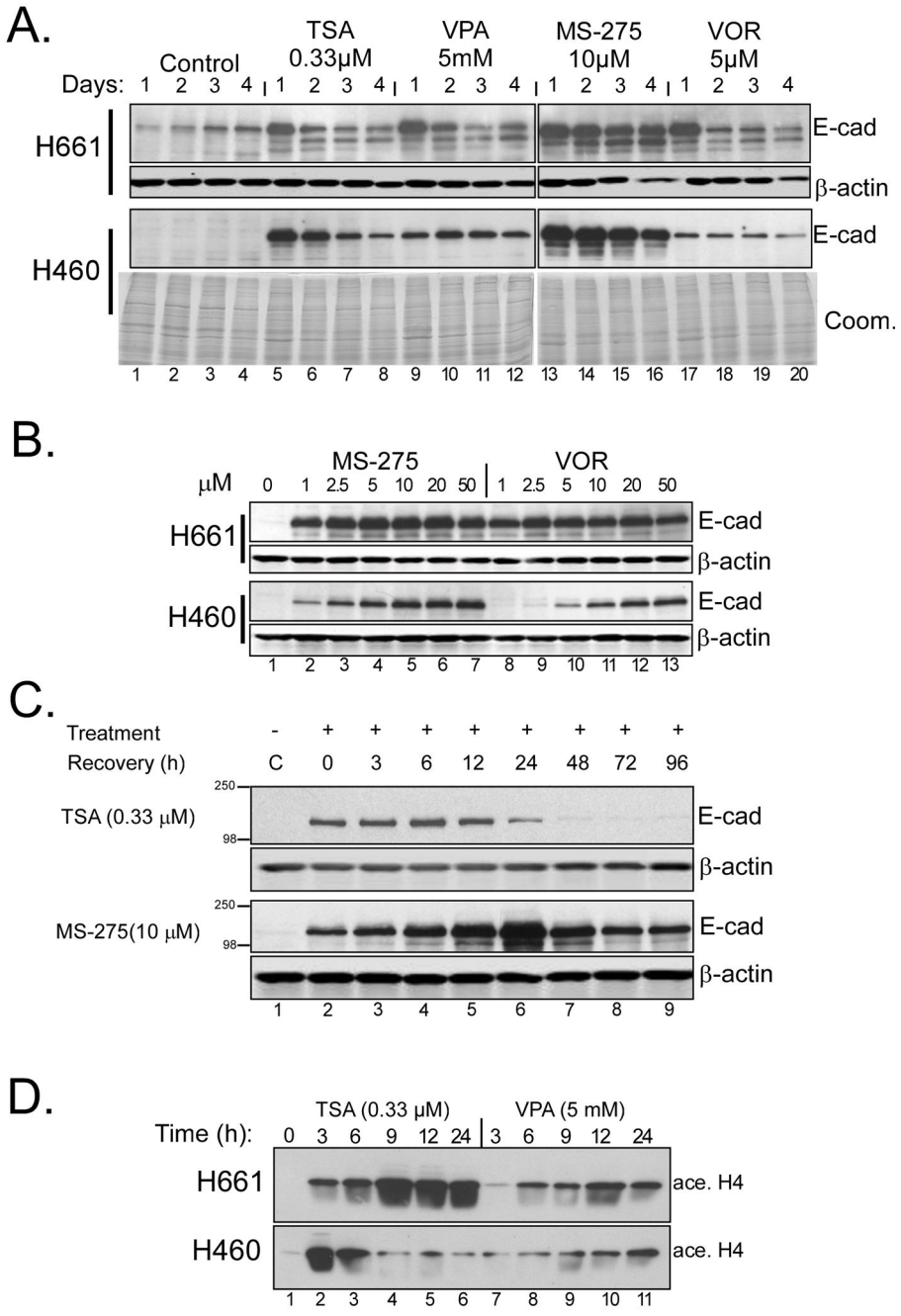

Figure 1. Induction of E-cadherin in NSCLC cell lines by HDAC inhibition

(A) Time course of E-cadherin induction in H661 and H460 cells with TSA, VPA, MS-275 and vorinostat (VOR). The indicated concentrations of each agent were added to cultures at time zero and samples taken over four days; agents were present throughout the time course. Equal aliquots of protein lysates were immunoblotted for E-cadherin. Equivalent loading was verified using anti-β-actin (H661) or Coomassie blue staining (H460, Coom.). (B) Dose-response to MS-275 and vorinostat. Cultures of H661 and H460 cells were treated with the indicated concentrations of MS-275 or vorinostat for 24 hours and analyzed for E-cadherin levels and actin. (C) Persistence of E-cadherin induction. H661 cells were treated with TSA or MS-275 for 12 hours followed by wash-out with fresh medium at zero time. Samples were

then harvested at the indicated time points and analyzed for E-cadherin and actin. (D) Time-course of acetylated histone H4 accumulation by HDAC inhibitors. H661 and H460 cells were treated with the indicated concentrations of TSA and VPA and samples analyzed for acetylated Histone H4 levels over time.

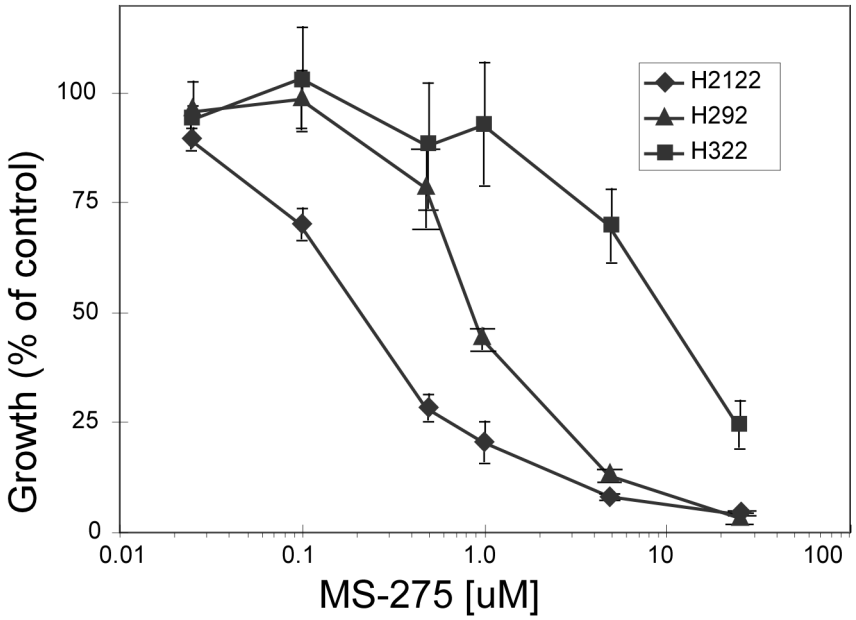

Figure 2. Growth inhibition following MS-275 treatment in NSCLC lines

MTT growth assays for three representative cell lines show the extreme responses among the panel of 12 NSCLCs tested. Cells were seeded into 96-well microtitre plates at between 2000 and 5000 per well. MS-275 was added from between 25 nM to 25 μM and treatment continued for 3 days. IC_{50} values for the complete cell line panel are provided in Table 1.

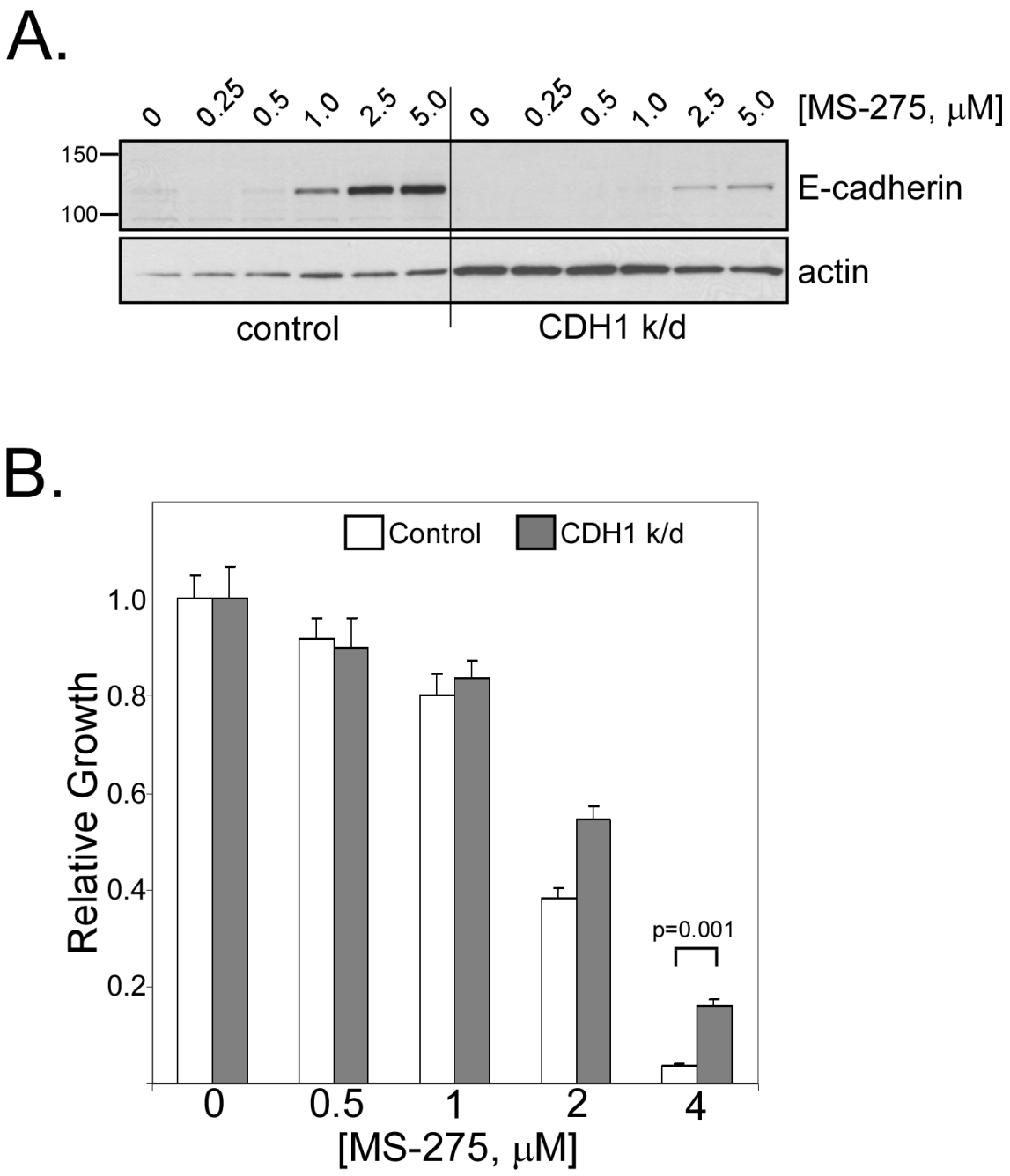

Figure 3. E-cadherin induction contributes to anti-proliferative effects of HDAC inhibition

(A) NCI-H661 cells were stably transfected with a shRNA construct targeting CDH1 mRNA or a non-targeting control. Transfected cells were tested for E-cadherin protein levels by Western blot after 24h MS-275 treatment using the indicated doses. (B) E-cadherin knock-down increased resistance to MS-275. MTT assays were performed on control and CDH1 knock-down H661 cells. Values are the average of two independent experiments, each performed in triplicate. Growth was significantly restored in CDH1 knock-down cells compared to controls when treated with 4 μM MS-275 ($p = 0.001$, Tukey's HSD test).

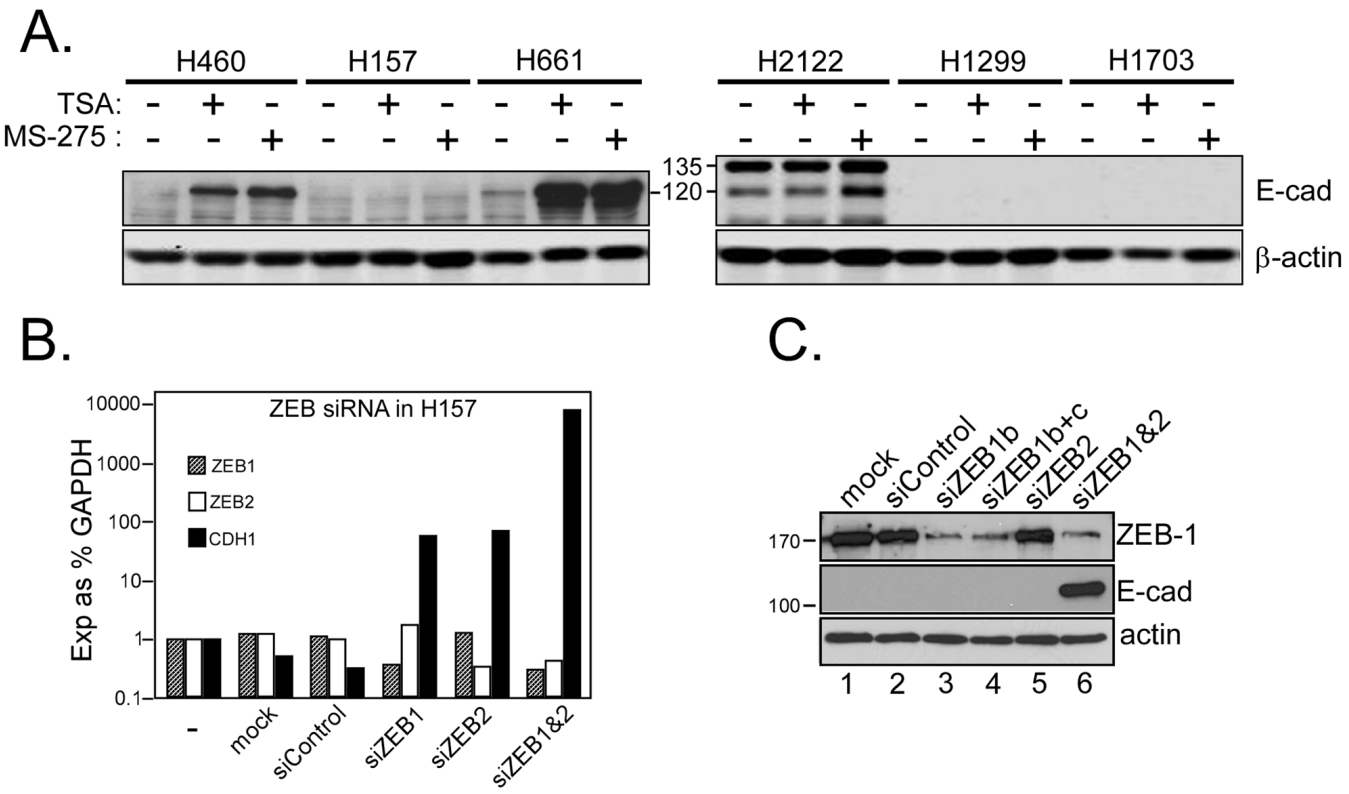

Figure 4. ZEB-1 and -2 inhibit E-cadherin in H157 cells in a HDAC class I/II independent manner

(A) Six NSCLC cell lines with negative or low E-cadherin expression were treated for 24h with TSA (0.33 μM) or MS-275 (5 μM). Protein lysates (10 μg) were analyzed for induced E-cadherin levels on Western blots. E-cadherin remained undetectable in H157, H1299 and H1703 cells after HDACi treatment. E-cadherin precursor (135 kDa) was observed only in H2122 (mature E-cadherin migrates at 120 kDa). (B) Synergistic induction of E-cadherin message by joint knockdown of ZEB-1 and -2. H157 cells were mock-transfected (mock), or transfected with control, ZEB-1 or ZEB-2-specific siRNAs, alone and in combination. Cells were harvested 48h post-transfection and processed for RNA and protein. ZEB-1, ZEB-2 and CDH1 were analyzed by realtime RT-PCR; bars are plotted as $\log_{10}$ of expression relative to GAPDH. (C) Protein samples from similarly treated cells were analyzed for ZEB-1 and E-cadherin on Western blots. ZEB-1-specific siRNA achieved substantial knockdown of protein (b, lane 3) but no further knockdown was observed upon addition of a second anti-ZEB-1 siRNA (b+c, lane 4). Knockdown of ZEB-2 was verified by realtime PCR since available anti-ZEB-2 antibodies were non-specific. E-cadherin was detectably induced only in cells knocked down for both ZEB-1 and -2 (lane 6).

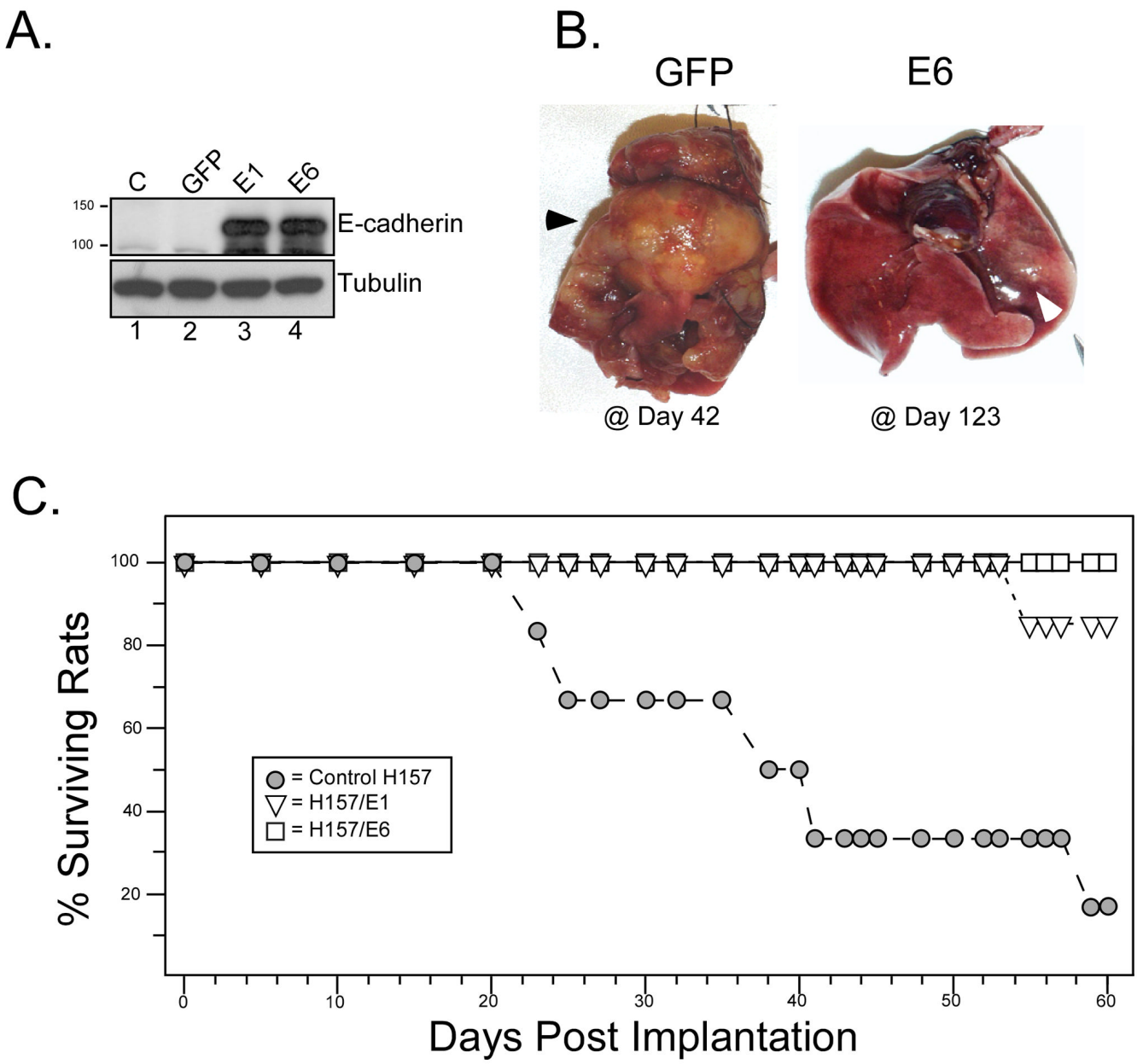

Figure 5. E-cadherin expression blocks tumorigenicity of NCI-H157 cells

(A) NCI-H157 cells were stably co-transfected with pEGFP-C1 and an E-cadherin expression construct (independent clones in lanes 3 and 4, pBATEM) or pEGFP-C1 alone (lane 2). Western blot for E-cadherin verified expression (top) while tubulin provided a loading control (bottom). (B) Orthotopic tumorigenicity assay. Ten million cells (H157/GFP controls or H157/E-cadherin transfectants) were introduced intra-tracheally into the left lung of irradiated athymic *nude* rats (6 per group), and tumor growth monitored for 60 days. H157 cells stably transfected with EGFP-C1 formed rapidly growing, metastatic tumors by 42 days post-inoculation (dark arrowhead). The E6 transfectant at 123 days had formed a typically small tumor (white arrowhead) in the left lung without metastasis. (C) Kaplan-Meier survival plots are shown for animals injected with the indicated transfectants (6 animals per group).

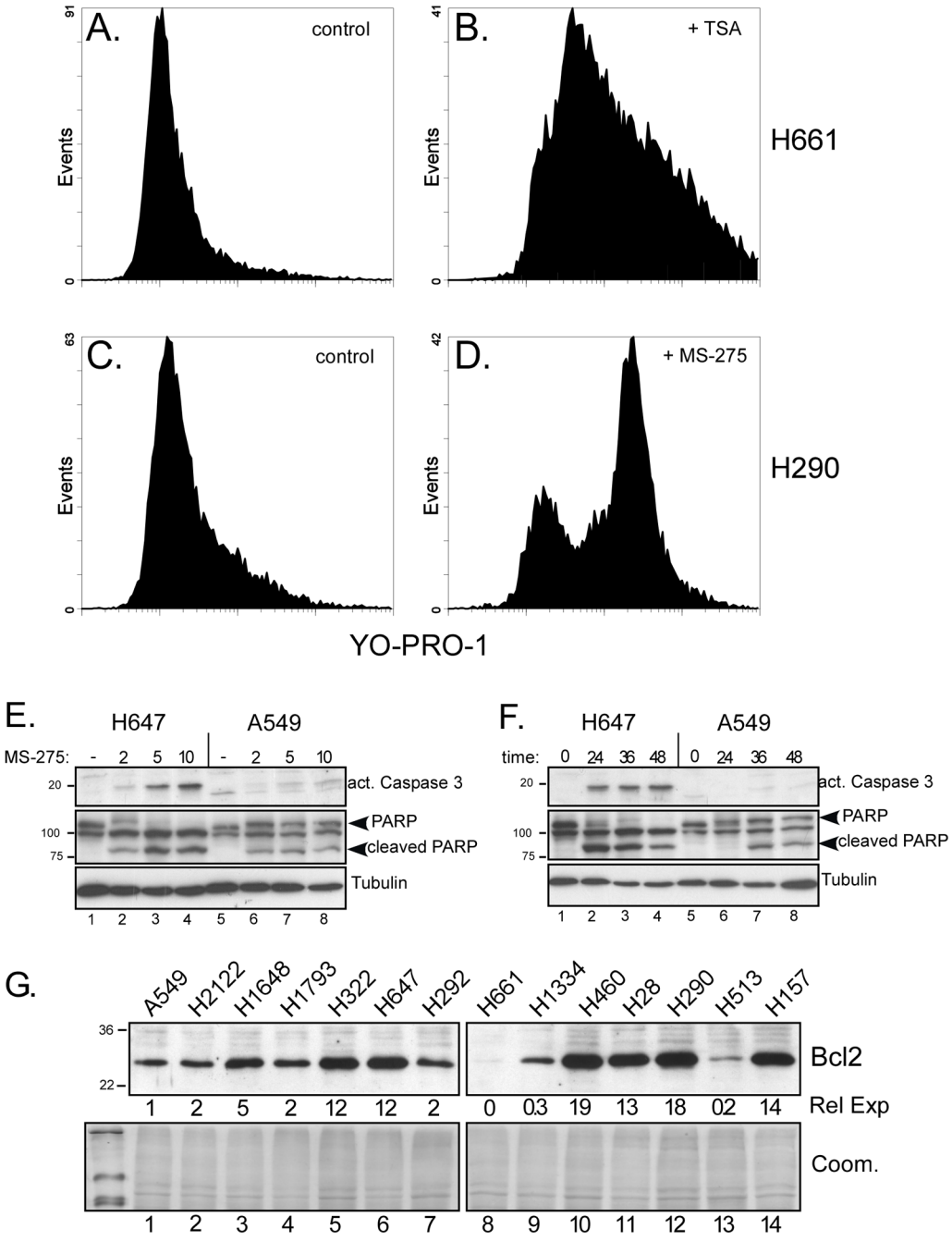

Figure 6. MS-275 induces apoptosis in NSCLC cell lines

(A–D) The indicated NSCLC cell lines were incubated with medium (controls), MS-275 (10 μM) or TSA (0.33 μM), as indicated, for 48 h. The percentage of apoptotic cells was determined by flow cytometry using dual staining with YO-PRO1 and propidium iodide. (A, C) Flow analysis of untreated control cultures for H661 (A) and H290 (C). (B, D) Flow analysis of H661 cells after treatment with TSA (B) and H290 cells after treatment with MS-275 (D). (E and F) MS-275 activates caspase-3 in sensitive NSCLC cell lines. (E, F) The moderately sensitive line H647 and the resistant line A549, were treated with MS-275 at different doses (E) or times (F) and examined for biochemical changes indicative of apoptosis. In (E), cultures were treated for 36 hours with the indicated doses of MS-275 (μM); in (F), cultures were treated

with 5 μM MS-275 for the indicated times. Lysates wereanalyzed by Western blot for activated caspase 3 and poly ADP ribose polymerase (PARP) cleavage. Tubulin provided loading controls. (G) Bcl-2 protein levels were measured in 14 NSCLC lines, as indicated. Signals from a shorter exposure (not shown) were densitized and normalized to the level obtained in A549 to yield relative expression (Rel Exp). A Coomassie stained gel (Coom.) provided a loading control.

Table 1

IC_{50} for MS275

	Cell line	IC_{50} [μM][1] MS275	Relative Bcl-2 exp	% Apoptotic[2] + MS275
Resistant	H322	9.18 +/−1.64	12	15 +/−1
	H1793	5.48 +/−1.19	2	nd
	A549	3.42 +/−0.92	1	5 +/−0
Moderate	H513	2.00 +/−0.6	0.2	36 +/−3
	H647	1.74 +/−0.31	12	59 +/−17
	H292	1.15 +/−0.24	2	32 +/−3
Sensitive	H290	0.79 +/−0.13	18	36 +/−17
	H157	0.75 +/−0.21	14	36 +/−13
	H460	0.55 +/−0.10	19	28 +/−7
	H1648	0.45 +/−0.15	5	nd
	H661	0.43 +/−0.12	0	40 +/−3
	H2122	0.26 +/−0.06	2	53 +/−10

[1] Values are means ± s.d. for 3 experiments, each done in triplicate

[2] Values for H322 and H2122 were done in duplicate

Table 2

17-AAG IC_{50} and combination Index with MS275

Cell Line	Histology	IC_{50} [μM][4] 17-AAG	IC_{50} [μM][4] MS275	*CI*	[MS275/17AAG] @ peak synergy
H647	ad-sq	0.449 +/−0.27	1.74 +/−0.31	0.51	0.5/0.05[3]
H322[1]	bac	0.393 +/−0.098	9.18 +/−1.64	0.33	1.0/0.05
H290	meso	0.323 +/−0.148	0.79 +/−0.13	0.45	0.75/0.5
H661	large	0.157 +/−0.474	0.43 +/−0.12	0.53	0.25/0.5
H1793	adeno	0.083 +/−0.02	5.48 +/−1.19	31.80	antagonistic
H513	meso	0.073 +/−0.024	2.00 +/−0.6	0.82	0.05/0.005
H292	mucoepi	0.067 +/−0.005	1.15 +/−0.24	0.42	0.1/0.1
H157	squamous	0.051 +/−0.013	0.75 +/−0.21	0.35	0.1/0.02
H1648	adeno	0.021 +/−0.009	0.45 +/−0.15	0.36	0.25/0.005
A549	adeno	0.021 +/−0.003	3.42 +/−0.92	0.64	2.5/0.001
H460	large	0.019 +/−0.003	0.55 +/−0.1	6.87	antagonistic
H2122[2]	adeno	0.011 +/−0.001	0.26 +/−0.06	0.31	0.01/0.05

[1] Seeded with 5000 cells per well

[2] Seeded with 4000 cells per well

[3] All concentrations listed as μM

[4] Values are means ± s.d. for 3 experiments, each done in triplicate

Table 3

Taxotere IC_{50} and combination Index with MS275

Cell Line	Histology	IC_{50} [μM][1] Taxotere	IC_{50} [μM][1] MS275	*CI*	[MS275/Tax] @ peak synergy
H647	ad-sq	0.00419 +/−.001	1.74+/−0.31	0.199	0.45/0.014
H322	bac	0.0029 +/−.00029	9.18 +/−1.64	0.441	0.45/0.014
H290	meso	0.065 +/−0.019	0.79 +/−0.13	0.197	0.4/0.05
H661	large	0.0031 +/−.0001	.43 +/−0.12	0.395	1.35/0.014
H1793	adeno	>0.150	5.48 +/−1.19	0.200	0.15/0.04
H513	meso	0.022 +/−0.014	2.00 +/−0.6	0.129	0.3125/0.005
H292	mucoepi	0.0024 +/−.0007	1.15 +/−0.24	0.244	0.15/0.014
H157	squamous	0.015 +/−0.005	0.75 +/−0.21	0.121	0.3125/0.005
H1648	adeno	0.0019 +/−0.0003	0.45 +/−0.15	0.080	0.45/.014
A549	adeno	0.022 +/−0.014	3.42 +/−0.92	0.216	0.3125/0.005
H460	large	0.010 +/−0.004	0.55 +/−0.1	0.553	5.0/0.05
H2122	adeno	0.025 +/−0.012	0.26 +/−0.06	0.265	0.15/0.005

[1]Values are means ± s.d. for 3 experiments, each done in triplicate